Available online at www.sciencedirect.com
SCIENCE DIRECT®
Journal of Membrane Science 253 (2005) 209–215
journal of MEMBRANE SCIENCE
www.elsevier.com/locate/memsci

Single component gas transport through 10 nm pores: Experimental data and hydrodynamic prediction

Subrata Roy [a], Sarah M. Cooper [b], M. Meyyappan [b], Brett A. Cruden [b,*]

[a] *Computational Plasma Dynamics Laboratory, Department of Mechanical Engineering, Kettering University, Flint, MI 48504, USA*
[b] *NASA Ames Research Center, Center for Nanotechnology, Moffett Field, CA 94035, USA*

Received 22 June 2004; received in revised form 12 November 2004; accepted 18 November 2004
Available online 25 February 2005

Abstract

This paper presents experimental measurements of argon and oxygen gas flow through a 10 nm polycarbonate membrane, which are an order of magnitude higher than would be predicted by Knudsen diffusion alone, but may be described as rarified diffusion with slip (Knudsen–Smoluchoski diffusion). We also simulate the Poiseuille gas flow using a finite element based model and find that the hydrodynamic model may successfully predict Knudsen-like diffusion for Knudsen numbers as high as 10, contrary to conventional wisdom about the limitations of continuum models in the rarified regime. With the addition of slip boundary conditions, the model is able to describe the data with a similar tangential momentum accommodation coefficient (TMAC) as predicted by Knudsen–Smoluchoski diffusion. Transient measurements show that the pressure decay can be expressed by two distinct time constants, both of which indicate a faster decay than predicted by the Knudsen–Smoluchoski relations. The fact that the hydrodynamic model can successfully predict measured flow characteristics while conventional Knudsen–Smoluchoski rarified gas transport fails demonstrates that the hydrodynamic model may be extended into the nanoscale regime even at low gas density.

Keywords: Knudsen–Smoluchoski relations; TMAC; Polycarbonate membrane; Hydrodynamic model; Slip boundary conditions

1. Introduction

Ultra permeable fluid transport properties have become pivotal for understanding flow through meso and nanoscale devices [1,2]. Traditionally, it has been argued [3,4] that the hydrodynamic model based on Navier–Stokes equation is valid only for low Knudsen numbers ($0 < Kn < 0.1$) and fails beyond an upper limit of slip flow. For example, a microchannel Poiseuille flow analysis [4] for Reynolds number between 1 and 400 used a finite volume based numerical model and assumed a tangential momentum accommodation coefficient (TMAC) value of unity could not recover the Knudsen diffusion regime and could not predict the hydrodynamic development length beyond $Kn = 0.1$. Recently, it has been shown [5] that for silica pores of radius 1.92 nm with diffusely reflecting walls, viscous flow is dominant at high density and a significant degree of slip controls the flow at low densities. The analysis also showed that for this confined cylindrical geometry at low densities ($<4\,\mathrm{nm}^{-3}$) the transport properties of single component subcritical Lennard–Jones (LJ) flow could be explained by hydrodynamic mechanisms alone. The constancy of the friction coefficient at the nanopore wall is noted [5] as an indicator of the dominance of slip flow. Thus, contrary to the reported limitation of hydrodynamic model [3,4], TMAC of unity should be able to successfully resolve the Knudsen flow solution, as will be shown here.

In recent papers [6,7] it has been shown that an accurate imposition of wall slip condition can extend the hydrodynamic model beyond the transitional flow regime. A combined experimental and hydrodynamic modeling approach was presented [6,7] to successfully characterize the significant deviation from diffuse scattering for various gas transports in nanopores and nanotubules. Argon transport in

* Corresponding author. Tel.: +1 650 604 1933; fax: +1 650 604 2459.
E-mail address: bcruden@mail.arc.nasa.gov (B.A. Cruden).

0376-7388/$ – see front matter © 2005 Elsevier B.V. All rights reserved.
doi:10.1016/j.memsci.2004.11.033

an anodic alumina membrane with a 200 nm diameter pore was successfully modeled [6] by describing the gas-wall interactions with a diffusive TMAC of $\sigma_v = 1$. The wall reflection becomes increasingly decollimated for amorphous carbon nanotubules of diameter 170 nm, in which a TMAC of $\sigma_v = 0.52 \pm 0.1$ best represented the experimental data obtained for argon, oxygen and nitrogen [7]. Recent simulation results [8] have shown significant deviation from diffuse scattering for pore sizes 20–100 Å, with the TMAC depending on the solid lattice and the fluid–solid interaction parameters. Further size reduction of the transport carrier may result in incorrect modeling of the shear stress and non-equilibrium processes. In such a case one can significantly alter predicted flow properties by controlling the nature of the pore surfaces [7] and possibly by modifying the bulk viscosity [9] and adding the quantum effect [10]. If the viscous effects are negligible, a comparison between equilibrium and non-equilibrium molecular dynamics (EMD/NEMD) analysis with dual control volume grand canonical molecular dynamics (DCV–GCMD) [11] shows that all three methods calculate the same transport coefficient in micropores.

This paper reports experimental measurements and hydrodynamic prediction of the characteristic behavior of gas flow through polycarbonate membranes (PCM) with pores of 10 nm diameter and infinitely thick walls. Here, as in our prior work, only the first order wall-gas interactions are used as control parameters and a TMAC significantly less than unity is found to effectively identify the transport properties of a single component gas flow through these pores. It is also shown for the first time that the hydrodynamic model successfully characterizes the unsteady pressure decay in these pore sizes.

2. Approach

The experimental setup and theoretical approach for flow characterization have been explained in a previous publication [6]. Experimental characterization is performed in a flow tube where pressure drop across the membrane is monitored versus a controlled flow rate. The membranes studied in this work are 6 μm thick commercially available polycarbonate membranes (Poretics) with 10 nm diameter pores at a density of $6.0 \times 10^{12}\ \mathrm{m}^{-2}$, giving a membrane porosity of 4.1×10^{-4}. Fig. 1 shows scanning electron micrograph (SEM) images of the membrane surface. In our previous experiments, uncertainty in the membrane porosity was the largest source of error in comparing the overall flow through the membrane to the simulation of transport through a single pore. For these membranes, the manufacturer reports a ±15% tolerance on pore density and +0, −20% tolerance on pore diameter, giving an uncertainty of +15%, −55% on the experimental flux. The theoretical approach is a finite element based hydrodynamic model incorporating Navier–Stokes equations with a first order slip boundary condition implemented for efficient prediction of bulk flow characteristics. The code uses fully implicit time steps with Newton–Raphson iteration procedure. The computational channel (pore) geometry is discretized using two-dimensional nine-noded biquadratic finite elements. The continuity and equation of state are solved for pressure and density respectively using the four corner nodes of the element. For velocity and temperature calculations, all nine nodes of the biquadratic element are used. The time step solution is declared convergent when the maximum relative norm of residual for each of the state variables (like density, velocity component) becomes smaller than a chosen convergence criterion. For each data set, a single parameter, the TMAC ($0.15 \le \sigma_v \le 1.0$), is adjusted to match the experimental behavior.

To examine the slip, we introduce a non-dimensional wall friction coefficient ψ using the local density ρ_0, and slip velocity u_0 determined at the wall ($r = r_0$) where the fluid–solid potential is minimum as:

$$\psi = \frac{\mu}{\rho_0 u_0^2} \left| \frac{\partial u_z}{\partial r} \right| \text{ at } r = r_0 \tag{1}$$

This dimensionless friction coefficient represents the balance of volume specific kinetic energy of the fluid at min-

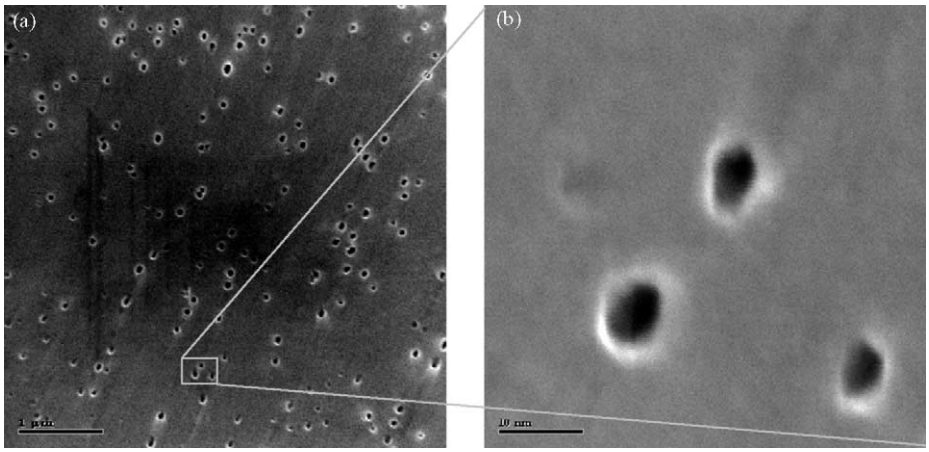

Fig. 1. SEM images of the polycarbonate membrane with 10 nm pore size: (a) looking end on at pore opening; (b) zoomed in view of a small area in (a).

imum potential with the shear due to wall slip. It differs from the friction coefficient in Ref. [5] which has an inertia imbedded within it. We have chosen this coefficient to reflect that the slip is limited by the kinetic energy (not the flux) of the fluid near the wall. The kinetic energy loss due to the diffuse momentum transfer at the slip wall can be described as $\psi\rho_0 u_0^2 = Zmu_0$, where $Z = \rho_0\sqrt{k_B T/2\pi m^{3/2}}$ is the surface collision frequency under local equilibrium. Upon utilizing the Bohm velocity $v_B = \sqrt{k_B T/2\pi m}$, the non-dimensional friction coefficient becomes $\psi = v_B/u_0$. We note that this is an important relation that may help identify flow characteristics in micro and nanoscale flows. One may also utilize the Navier slip condition into Eq. (1) and show that $\psi = \mu/L_s\rho_0 u_0 = \sigma_v\mu/(2-\sigma_v)\lambda\rho_0 u_0$, where L_s is the shear rate dependent slip length and λ is the fluid mean free path.

We have also measured the transient permeability of the nanoporous system for a single component fluid. This experiment is analogous to the initial flow method for estimating membrane permeability [12]. In short, the upstream volume is pressurized while the downstream volume is continually evacuated by a rotary pump, so that a steady flow through the membrane is obtained. The upstream volume is then closed from the gas source and the decay in pressure differential across the membrane is observed versus time. This case is simulated by utilizing unsteady fully implicit time integration procedure to attain the final pressure drop across the pore. For simulating the transient through a single pore, a closed upstream volume is added to the inlet side of the pore and the downstream end is kept open to let the gas leak out. To match the experiment, the additional closed volume is determined to be 1.35×10^{-13} m^3, based on the total upstream volume of about 1.92×10^{-4} m^3 for approximately 1.41×10^9 pores. Assuming ideal gas law this leakage flow is governed by the Reynolds transport theorem as, $(1/RT)(\partial/\partial t)\int_V P\,\mathrm{d}V + \rho u A_{sect} = 0$, where R is the universal gas constant, T is the Kelvin temperature of gas, P is the pressure, ρ is the density, u is the streamwise velocity, the cross-sectional area is A_{sect} and V is the upstream volume of the pipe. Thus, for an average length $\ell = V/A$, the pressure decay is $\partial P/\partial t = -\rho RTu/\ell$, i.e. $\mathrm{d}P/P = -(u/\ell)\,\mathrm{d}t$. Upon integration and rearrangement, this yields the pressure decay relation as

$$P = \exp\left(-\int\left(\frac{u}{l}\right)\mathrm{d}t\right) = A\exp\left(-\frac{t}{\tau_{eff}}\right) \quad (2)$$

where τ_{eff} is the effective time constant, which is a function of the streamwise velocity entering the pore and, contrary to a strictly diffusive transport regime, is not a constant value, as will be shown. At $t = 0$, the pore is given the profile of a fully developed steady flow, with the upstream volume at a constant pressure and the outlet at a very small pressure. Then, the simulation is allowed to run. There are no upstream boundary conditions, since it is a closed volume, flow may pass from that volume through the pore, but nowhere else. The downstream boundary condition is maintained at a constant, effectively zero, pressure.

3. Results

Fig. 2 shows the steady state experimental data obtained for argon and oxygen gas flow rate against maintained pressure drop. Also shown is the case of Knudsen diffusion, which underestimates the transport rate significantly (e.g. in [7]). The analytical equations for Hagen–Poiseuille flow in a cylinder (not shown) would underestimate the molar flux by two orders of magnitude. If we invoke the Knudsen–Smoluchowski formula to model the system as rarified flow with specular reflection, so that effective diffusivity is given by $D = D_K((2-\sigma_v)/\sigma_v)$, we can estimate a TMAC of approximately 0.21 for both argon and oxygen. This means that the gas particles will be reflected from the wall with 79% of the incident momentum while 21% of the incident momentum will be lost to the wall.

Fig. 3a benchmarks the numerical prediction for oxygen gas flux through the 10 nm pore with experimental data. The model was run for four different pressure drops of $\Delta p = 14.1$ kPa (106 Torr), 45.3 kPa (340 Torr), 84.0 kPa (630 Torr) and 149.5 kPa (1121 Torr). Consideration of rough wall with diffused reflection, i.e. $\sigma_v = 1.0$, has produced very low values and is shown as a reference dotted line at the bottom of the picture. It is noteworthy that this case accurately predicts the Knudsen diffusion regime, overlaid on the plot. Decreasing the slip coefficient dramatically increases the flux. For example, for $\Delta p = 14.1$ kPa (106 Torr), the mass flux is 1.9 mol/m^2 s with $\sigma_v = 1.0$ while for $\sigma_v = 0.15$ it is 23.5 mol/m^2 s. This results from a low resistance generated near the wall due to near specular reflection of the fluid particles. We estimate the wall accommodation coefficient to be 0.28 ± 0.1 for the most reasonable match with the data. This number is comparable to that obtained in the Knudsen–Smoluchowski approximation, albeit slightly

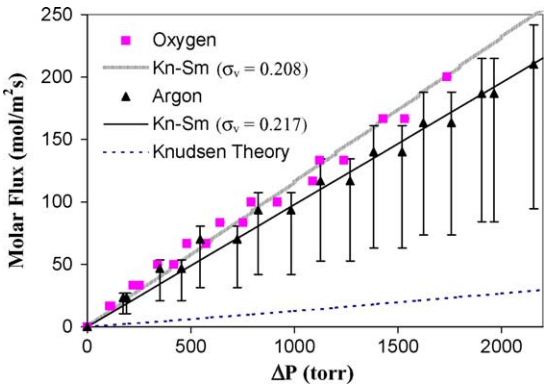

Fig. 2. Experimental measurement of molar flux vs. pressure drop. The data is fit with a Knudsen–Smoluchoski model and yields similar TMAC for both argon and oxygen. For comparison, the basic Knudsen diffusion model is shown to underestimate molar flux significantly.

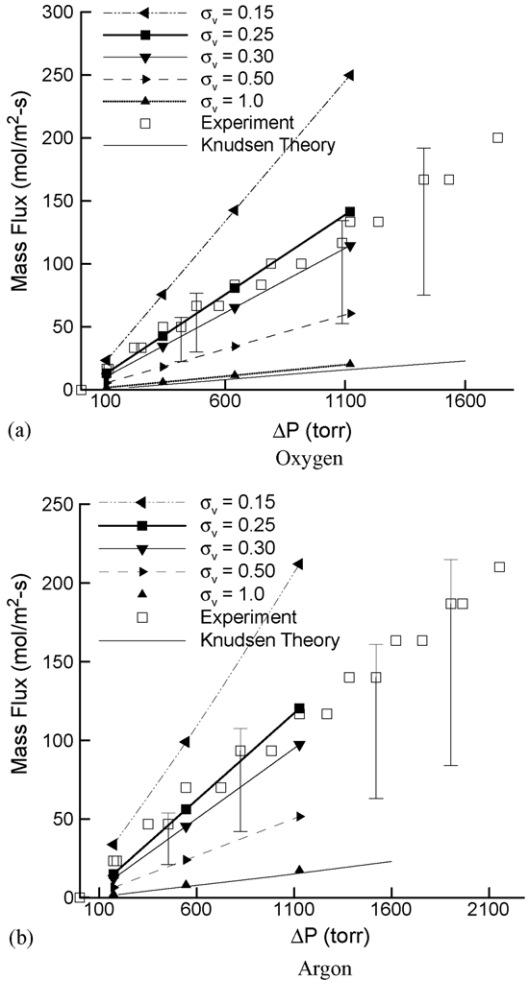

Fig. 3. Comparison of experimental data for molar flux vs. pressure drop with model results overlayed for a variety of TMAC values. The experimental uncertainty is shown on every fourth data point for clarity. The theoretical Knudsen relationship for transport is shown to match the model results for $\sigma_v = 1.0$. (a) For oxygen and (b) for argon.

larger. Qualitatively, all three of the model, experiment, and Knudsen–Smoluchowski give linear pressure-flow relationships. A similar trend is observed for argon gas in Fig. 3b where calculated flux is compared with data for three different pressure drops across the membrane ($\Delta p = 23.1$ kPa (173 Torr), 72.7 kPa (545 Torr) and 150.3 kPa (1127 Torr)). Again, the numerical prediction for $\sigma_v = 0.28 \pm 0.10$ represents the flow data well within the experimental uncertainty.

As representative data, Fig. 4a plots the essentially one-dimensional streamwise steady flow characteristics across the pore for oxygen gas with $\Delta p = 149.5$ kPa (1121 Torr). At the pore entrance, where flow is in the transition regime ($Kn < 10$), viscous effects are visible and the velocity profile is slightly parabolic. Near the end of the channel, where Knudsen number is large, the profile is flat (radially independent) indicating that viscous effects are not impacting the flow in this range. One concern with using the continuum model is that the concept of viscosity loses any physical meaning under a rarified flow regime. The absence of significant viscous effects in the solution in this regime minimizes this problem. The corresponding crosswise velocity in Fig. 4b is radially antisymmetric and small ($\sim 10^{-6}$ m/s). The streamwise velocity distribution at the centerline as plotted in Fig. 4c shows node locations where numerical computations were performed. The solution prediction remains flat at about 2 m/s across the pore before shooting up beyond the midsection from 2 to 33 m/s. This is due to the rapid increase in flow Knudsen number making the flow range from transition to free molecule as the density reduces across the pore as seen in Fig. 4d. Computed flow Reynolds number across the pore holds nearly a constant 0.001 confirming mass conservation.

The distribution of ψ at 29 equidistant points along the streamwise direction as shown in Fig. 4e depicts a near constant slope in friction factor for this very low density. The non-dimensional coefficient ψ shows a linear growth in fluid velocity as the ratio of thermalized Bohm velocity to fluid velocity at minimum potential decreases from 15 to 1, indicating significant slip constancy for this range of density. In the inset we plot the dimensional friction coefficient [5], which remains constant below and above a critical density but shows discontinuity at about 0.0085 nm^{-3}. A corresponding small change in slope for ψ is also noticeable for this low density indicating a sudden reduction in wall friction. This underscores the need for improved order modeling of wall parameters at this free molecule flow condition.

Fig. 5 shows the transient pressure decay measurement for oxygen. It is apparent that the pressure decay is not well described by a single exponential decay constant, as would be expected based on the analytical formalisms for Knudsen or Knudsen–Smoluchowski diffusion. For a total pressure drop of up to 273.2 kPa (2049 Torr), the decay is, in fact, best described by two time constants, an initial slow time constant ($\sim$820 s) observed for pressure above 80 kPa ($\sim$600 Torr), and a faster time constant ($\sim$318 s) for pressures below 7 kPa ($\sim$50 Torr). Both of these time constants are much faster than would be expected in the Knudsen diffusion regime ($\sim$8100 s). In Knudsen–Smoluchoski diffusion, this would require two different TMACs, a high pressure TMAC of 0.18 and a low pressure TMAC of 0.075. This behavior does not reconcile with the static diffusion behavior, suggesting a more complicated picture than can be described by straightforward Knudsen–Smoluchoski diffusion. A rarefied diffusion model is not appropriate to this system because the Knudsen number is varying as a function of both time and position and is not always in a molecular flow regime. A better match to experiment is obtained by applying the hydrodynamic model with slip boundary conditions. The computational prediction of this process is overlaid in Fig. 5, comparing the computed unsteady pressure decay for oxygen with the experimental data. Due to numerical difficulties, a lower initial pressure 149.5 kPa (1121 Torr) was used for simulation, however still

shows the same behavior. The hydrodynamic model also predicts two distinct time constants, an initial slow time constant (∼982 s) for pressure above 70 kPa (∼500 Torr) and a faster time constant (∼285 s) for pressures below 7 kPa (∼50 Torr). These time constants differ somewhat from the experimental data but are still within 20% of the measurement. This difference may stem from the variation in the experimental pore density and diameter, however the qualitative similarities suggest that the correct physics are included. While we have empirically assigned two time constants, in reality the system is never in an exponential decay regime. The apparent ("effective") time constant is given as:

$$\tau_{\text{eff}} = P\left(\frac{\mathrm{d}P}{\mathrm{d}t}\right)^{-1} \tag{3}$$

And from (2) we find this to be $\tau_{\text{eff}} = V/A\langle u\rangle$, where $\langle u\rangle$ is the time-averaged upstream velocity. As this velocity changes with time, particularly as the flow transitions from a transitional to free molecular flow regime, the effective decay constant will be time dependent.

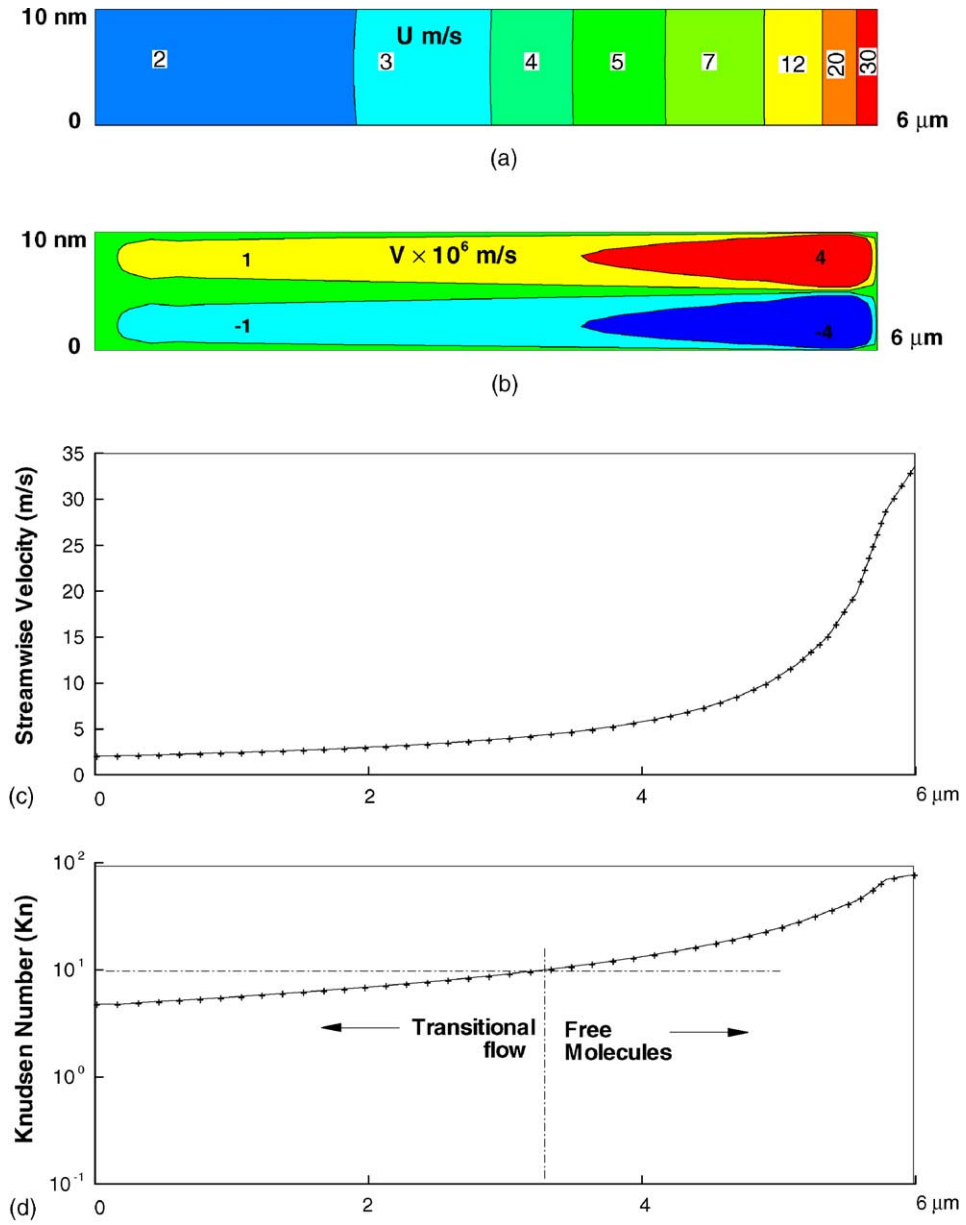

Fig. 4. Representative steady pore flow simulation result demonstrates an essentially one-dimensional characteristics for oxygen gas with $\Delta p = 149453.962$ Pa (1121 Torr). (a) Streamwise flow velocity, (b) crosswise flow velocity, (c) centerline distribution of streamwise flow shows sharp increase downstream, (d) centerline Knudsen number distribution based on pore diameter shows that the flow ranges from transition to free molecule regime, (e) non-dimensional friction coefficient plotted against density at potential minimum shows a constant slope. The inset shows the discontinuity of dimensional friction coefficient [5] at a very low critical density.

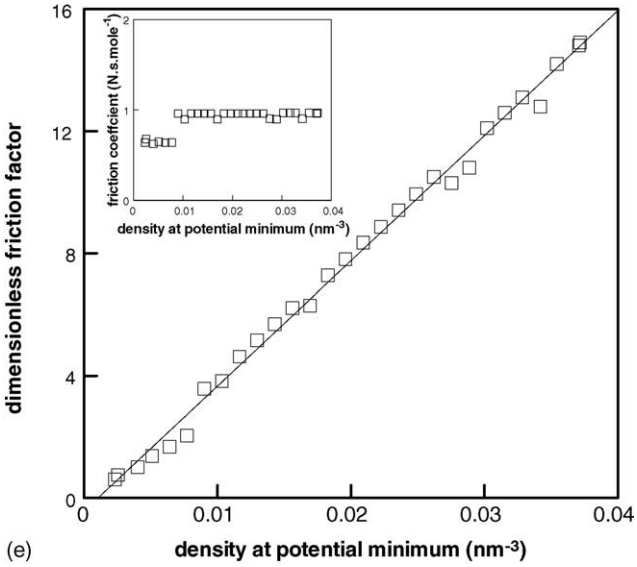

Fig. 4. (*Continued*).

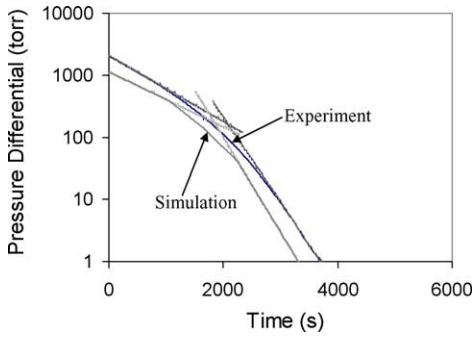

Fig. 5. Predicted pressure evolution for $\sigma_v = 0.25$ is benchmarked with experimental data for oxygen. Lines overlaid represent single exponential fits of different sections of the data.

4. Conclusions

In conclusion, we have used experimental data and theoretical modeling to estimate the slip coefficient for 10 nm PCM. The TMAC was predicted to be as low as 0.28 ± 0.1, which allows for a much higher throughput through the pore than would be predicted by a classical rarified diffusion or hydrodynamic flow case with no-slip boundaries. This number is somewhat lower than that found for 170 nm diameter pores with amorphous carbon coating on the surface [7]. In contrast, the MD results of Skoulidas et al., for 8 and 13 nm diameter carbon nanotubes estimate diffusivities that are about two orders of magnitude higher than Knudsen diffusivities, implying their slip coefficient would have to be significantly less than that estimated in this work [2]. A new non-dimensional friction coefficient has been defined at the position of minimum fluid–solid potential. Interestingly, in the regime of our study ($<0.04\,nm^{-3}$) this friction coefficient decreases linearly with the local density where the fluid–solid potential is minimum. Transient pressure decay data shows that the rate of flow through the pore increases as the pressure drops, and is not in an exponential decay regime, though it is possible to determine at least two empirical exponential time constants for decay in different pressure regimes. These constants are an order of magnitude smaller than the diffusive Knudsen decay constant and are also less than the time constants predicted based on steady state Knudsen–Smoluchoski diffusion rates. This experimental data is corroborated by the hydrodynamic model with slip boundary conditions. The fact that this data is well described by the hydrodynamic model while conventional rarified gas models fail suggests that it is possible to successfully extend continuum models into the nanoscale transport regime. However, further confirmation of the validity of the continuum model with a statistical particle-based model on the same system would be desired, and is a direction for future work in this area.

Acknowledgements

For this work, Sarah Cooper was supported by the NASA Ames Educational Associates program. Brett Cruden performed this work under NASA contract NAS2-99092 to Eloret Corporation. Subrata Roy was partially supported by AFRL contract no. F33615-98-D-3210 and NASA grant NAG3-2520. Authors acknowledge help from Reni Raju of George Washington University.

References

[1] T.C. Merkel, B.D. Freeman, R.J. Spontak, Z. He, I. Pinnau, P. Meakin, A.J. Hill, Ultrapermeable, reverse-selective nanocomposite membranes, Science 296 (2002) 519.
[2] A.I. Skoulidas, D.M. Ackerman, J.K. Johnson, D.S. Sholl, Rapid transport of gases in carbon nanotubes, Phys. Rev. Lett. 89 (2002).

[3] M. Gad-el-Hak, The fluid mechanics of microdevices – The Freeman Scholar Lecture, J. Fluids Eng., Trans. ASME 121 (1999) 5.
[4] R.W. Barber, D.R. Emerson, The influence of Knudsen number on the hydrodynamic development length within parallel plate microchannels, in: M. Rahman, R. Verhoeven, C.A. Brebbia (Eds.), Advances in Fluid Mechanics IV, WIT Press, Southampton, UK, 2002, p. 207.
[5] S.K. Bhatia, D. Nicholson, Hydrodynamic origin of diffusion in nanopores, Phys. Rev. Lett. 90 (2003) 16105.
[6] S. Roy, R. Raju, H.F. Chuang, B.A. Cruden, M. Meyyappan, Modeling gas flow through microchannels and nanopores, J. Appl. Phys. 93 (2003) 4870.
[7] S.M. Cooper, B.A. Cruden, M. Meyyappan, R. Raju, S. Roy, Gas transport characteristics through a carbon nanotubule, Nano Lett. 4 (2004) 377.
[8] G. Arya, H.C. Chang, E.J. Maginn, Molecular simulations of Knudsen wall-slip: effect of wall morphology, Mol. Simul. 29 (2003) 697.
[9] W.E. Meador, G.A. Miner, L.W. Townsend, Bulk viscosity as a relaxation parameter: fact or fiction, Phys. Fluids 8 (1996) 258.
[10] C.L. Gardner, The quantum hydrodynamic model for semiconductor-devices, SIAM J. Appl. Math. 54 (1994) 409.
[11] G. Arya, H.C. Chang, E.J. Maginn, A critical comparison of equilibrium, non-equilibrium and boundary-driven molecular dynamics techniques for studying transport in microporous materials, J. Chem. Phys. 115 (2001) 8112.
[12] B.A. Cruden, M. Meyyappan, Corrected equations for membrane transport characterization by manometric techniques, J. Membr. Sci. 221 (2003) 47.